Time scales of membrane fusion revealed by direct imaging of vesicle fusion with high temporal resolution

Christopher K. Haluska*†, Karin A. Riske*‡, Valérie Marchi-Artzner§¶, Jean-Marie Lehn§, Reinhard Lipowsky*, and Rumiana Dimova*‖

*Max Planck Institute of Colloids and Interfaces, Science Park Golm, 14424 Potsdam, Germany; and §Laboratoire de Chimie des Interactions Moléculaires, Collège de France, 75005 Paris, France

Edited by Harden M. McConnell, Stanford University, Stanford, CA, and approved September 2, 2006 (received for review April 6, 2006)

Membrane fusion is a vital process of life involved, for example, in cellular secretion via exocytosis, signaling between nerve cells, and virus infection. In both the life sciences and bioengineering, controlled membrane fusion has many possible applications, such as drug delivery, gene transfer, chemical microreactors, or synthesis of nanomaterials. Until now, the fusion dynamics has been elusive because direct observations have been limited to time scales that exceed several milliseconds. Here, the fusion of giant lipid vesicles is induced in a controlled manner and monitored with a temporal resolution of 50 μs. Two different fusion protocols are used that are based on synthetic fusogenic molecules and electroporation. For both protocols, the opening of the fusion necks is very fast, with an average expansion velocity of centimeters per second. This velocity indicates that the initial formation of a single fusion neck can be completed in a few hundred nanoseconds.

electrofusion | fast digital microscopy | liposomes | membrane biophysics | molecular recognition

Membrane fusion is a ubiquitous process of life. A prominent example is provided by the fusion of synaptic vesicles to the outer membranes of nerve cells. This fusion results in the release of neurotransmitters into the synaptic cleft and is thus responsible for nerve cell communication. Likewise, fusion is essential for other secretion processes based on exocytosis, for the intracellular traffic of transport vesicles, and for the infection by membrane-enclosed viruses. Furthermore, control of lipid bilayer fusion is desirable in a number of applications in the life sciences. Fusion of functionalized lipid vesicles with cell membranes could be used for advanced drug delivery and gene transfer. Fusion of vesicles containing different reactants provides chemical microreactors with rather small volumes in the picoliter range (1, 2). Fusion of membranes that differ in their composition could also be used to elucidate the character and size of intramembrane domains and rafts (3). Although three-component lipid membranes exhibit large intramembrane domains (4–7) that can grow up to many micrometers, the size and character of analogous domains within biological membranes is still controversial.

The fusion of two bilayer membranes is believed to proceed via several stages (8, 9): membrane proximity and contact, local perturbation of bilayer structure, formation of fusion pores or necks, and subsequent expansion of these necks. Snapshots of single fusion necks with a diameter of 50–100 nm have been obtained by electron microscopy (10) and corroborated by atomic force microscopy (11). The time period between local bilayer perturbation and completion of a single fusion neck can be rather short as follows from electrophysiological methods applied to the fusion of small vesicles with cell membranes (12–14). The time evolution of the observed membrane capacitance, which is proportional to the total membrane area, indicates that the formation of the fusion neck is presumably faster than 100 μs. However, for both biological and biomimetic model membranes, direct imaging of the fusion neck dynamics with this temporal resolution has not been reported so far. Even though electron microscopy produces detailed images of fusion products, it gives only single snapshots of frozen or stained samples (10, 15). Likewise, scanning force microscopy (11) and x-ray diffraction (16) can provide only static images of structures immobilized on a substrate surface. The most promising technique for direct imaging of the dynamics of lipid bilayer fusion is optical video microscopy (17). Until recently, this technique has been limited to conventional video frequencies or millisecond resolution. In the present study, we used a fast digital camera to record the fusion process directly with a time resolution of 50 μs, which is only feasible if fusion is induced in a controlled manner. We used two different protocols of controlled fusion, one based on synthetic fusogenic molecules (18) and the other on electroporation (19–21).

In the living cell, the fusion process is controlled and regulated by many proteins such as membrane-anchored soluble *N*-ethylmaleimide-sensitive factor attachment protein receptors (SNAREs) (22–25) and protein phosphatase (26). The conformational changes of these proteins are believed to induce and assist the formation of a fusion pore or neck (8) by bringing the membranes into close proximity and locally perturbing the two adjacent lipid bilayers. Recently, the action of fusion proteins has been mimicked by synthetic ligand molecules that are connected to lipid-like membrane anchors (18, 27). In the present study, we used amphiphilic ligands with a β-diketone head group that can be cross-linked by Eu^{3+} ions (28).

Results

To induce fusion of the lipid bilayer in a controlled manner, two lipid vesicles functionalized with the β-diketone ligand molecules (the chemical structure is provided in Scheme 1, which is published as supporting information on the PNAS web site) were isolated and brought into close proximity by using two micropi-

Author contributions: C.K.H. and K.A.R. contributed equally to this work; R.L. and R.D. designed research; C.K.H. and K.A.R. performed research; V.M.-A. and J.-M.L. contributed new reagents/analytic tools; C.K.H., K.A.R. and R.D. analyzed data; and R.L. and R.D. wrote the paper.

The authors declare no conflict of interest.

This article is a PNAS direct submission.

Freely available online through the PNAS open access option.

Abbreviation: fps, frames per s.

†Present address: Institut Charles Sadron, Centre National de la Recherche Scientifique, 67083 Strasbourg, France.

‡Present address: Instituto de Física da Universidade de São Paulo, CEP 05508-090 São Paulo, Brazil.

¶Present address: Synthèse et Electrosynthèse Organiques, Unité Mixte de Recherche 6510, Centre National de la Recherche Scientifique, Université de Rennes 1, Bât 10A, 35064 Rennes, France.

‖To whom correspondence should be addressed. E-mail: dimova@mpikg.mpg.de.

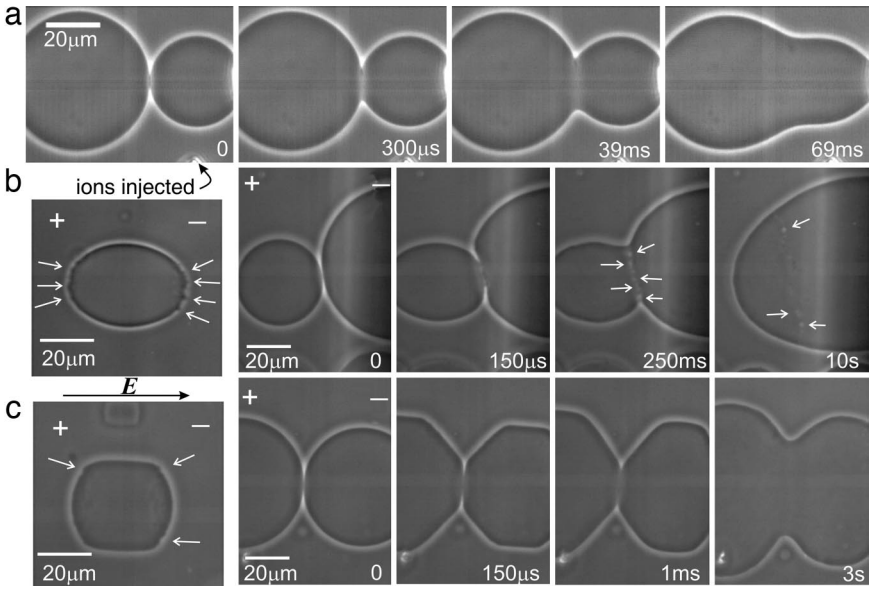

Fig. 1. Several series of snapshots for the fusion of two vesicles. (*a*) Fusion of two functionalized vesicles (of radii 25.4 and 16.6 μm) held by micropipettes (only the right pipette tip is visible on the snapshots). A third pipette (bottom right corner) is used to inject a small volume (few tens of nanoliters) of 50 μM solution of $EuCl_3$. The first image corresponding to the starting time $t = 0$ represents the last snapshot before the adhesion zone of the vesicles undergoes detectable changes. (*b*) The behavior of a single vesicle (first image) and a vesicle couple (remaining images) when exposed to a dc pulse in the absence of salt. The amplitude of the dc pulse was 90 V (1.8 kV/cm), and its duration was 150 μs. (*c*) Behavior of a single vesicle (first image) and a vesicle couple (remaining images) in the presence of 1 mM NaCl in the exterior solution (the vesicle radii are 29.0 and 26.5 μm). In this case, the amplitude of the dc pulse was 150 V (3 kV/cm), and its duration was 150 μs. The polarity of the electrodes is indicated with a plus (+) or a minus (−) sign. The arrows in the first images indicate porated parts of the membrane, which lead to the leakage of enclosed liquid. For both *b* and *c*, the starting time $t = 0$ corresponds to the beginning of the dc pulse. In the last two snapshots of the sequence (*b*), the fused vesicles contain an array of internal vesicles (bright spots) as indicated by the arrows. The image acquisition rate was 20,000 fps. For more details, see Movies 1–4.

pettes. To do so, we first prepared a large number of vesicles by using electroformation as described in *Methods*. From this preparation, we carefully selected two unilamellar vesicles, which had no visible defects, and brought them together via the micropipettes. Then a third micropipette was used to inject a small volume of $EuCl_3$ solution into the contact zone between the two vesicles (see Fig. 1*a*). This procedure was applied to ≈100 vesicle couples, half of which ruptured within a few seconds after the ion injection. For the remaining 50 couples, we observed five successful fusion events, three of which have been recorded by a CCD camera with 28 frames per s (fps) and two by the fast digital camera with 20,000 fps (see Movies 1 and 2, which are published as supporting information on the PNAS web site).

The delay time between the injection of $EuCl_3$ and the beginning of the fusion process was governed by a broad distribution of times between 1 and 5 min. It is not feasible, at present, to record such a time period with 50-μs resolution because it would require between 120 and 600 gigabytes of on-board memory storage in the digital camera. We used a camera with 4 gigabytes on-board memory, which allows storing an image sequence of 2 s consisting of 40,000 frames. Thus, to capture a fusion event with the fast digital camera, we had 2 s to visually notice it and stop the camera from erasing its memory.

For comparison, we also studied the dynamics of electrofusion with the same temporal resolution (see Fig. 1 *b* and *c*). In the latter case, the delay time between the applied electric pulse and the beginning of the electrofusion process is only a fraction of a millisecond, much shorter than for the ligand-mediated case, and thus, easier to record with the fast camera (see Movies 3 and 4, which are published as supporting information on the PNAS web site).

Applying both ligand-mediated fusion and electrofusion, we identified two different dynamic regimes. During the first 300 μs, the fusion necks opened very rapidly, expanding with an average velocity of centimeters per second for both protocols. This result was surprising because the initial molecular rearrangements were expected to be rather different for the two types of fusion protocols (see Fig. 2). After 300 μs, the expansion of the fusion neck slowed down by approximately two orders of magnitude. Despite the differences between the two fusion protocols, the

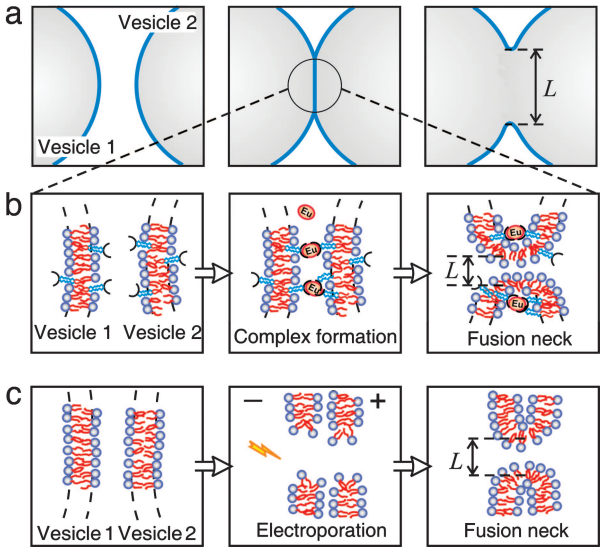

Fig. 2. Molecular mechanisms of membrane fusion. (*a*) The fusion process as observed on the micrometer scale (compare Fig. 1). (*b* and *c*) The cartoons in *b* and *c* are hypothetical molecular rearrangements for ligand-mediated fusion (*b*) and electrofusion (*c*), which we might see if we were able to zoom into the contact zone with molecular resolution.

dynamics of the fusion neck opening was, in fact, found to be quite similar as explained in the following sections.

First Protocol: Ligand-Mediated Fusion. In the first fusion protocol, we used giant unilamellar vesicles made of conventional lipid–egg phosphatidylcholine (egg-PC) or lecithin. We functionalized these egg-PC vesicles by incorporating lipid-like molecules with β-diketone "head groups" (28). A micropipette was used to inject a solution of $EuCl_3$ locally over a population of vesicles or directly into the area of contact between two giant vesicles that were trapped and displaced by two additional micropipettes (see Fig. 1*a*). When injected over vesicles in contact, $EuCl_3$ induced adhesion. In addition, Eu^{3+} is known to form a coordination complex with β-diketone groups in a 1:2 ion-to-ligand ratio (28). When the complex of one europium ion and two or more ligands is formed between two adjacent membranes, fusion is triggered (a possible mechanism for this interaction on the molecular level is shown in Fig. 2*b*). In contrast, in the absence of the β-diketone groups, nonspecific interaction between the lipid molecules in the membrane and Eu^{3+} induced adhesion but no fusion. No significant dependence on the ligand concentration, the $EuCl_3$ concentration, or the membrane tension applied with the pipettes was observed (see *Methods* for details).

Second Protocol: Electrofusion. The second fusion protocol is based on electroporation. Initially, the ac field can be used to bring two vesicles into contact and align them in the field direction [an effect similar to the one observed with cells where the latter align in the field direction in pearl chains (19)], after which a dc pulse is applied. The effect of dc pulses on single vesicles has been reported in detail (29). Briefly, the vesicle shapes are deformed by the transmembrane potential, which arises from the applied pulse. In the absence of salt, the vesicles attain a prolate shape (see the first snapshots in Fig. 1*b* and Movie 3). When the solution outside of the vesicles contains a small amount of salt ($\approx$1 mM NaCl), unusual short-lived shape deformations, mainly cylindrical, are observed (see the first snapshots in Fig. 1*c*). Although intriguing, the nature of these morphological changes is not the main focus of the present study and is discussed elsewhere (30). When the applied transmembrane potential exceeds some critical value, it porates the membranes (see arrows on the first snapshots in Fig. 1 *b* and *c*). The minimal pore radius that can be observed in this way is $\approx$0.5 μm.

Applying the dc pulses to a couple of vesicles brought into contact leads to fusion (see the series of snapshots in Fig. 1 *b* and *c* and Movies 3 and 4). On the molecular scale, the formation of the fusion neck is likely to proceed via the steps shown in Fig. 2*c*. Membrane poration is a necessary condition for vesicles in contact to fuse. Thus, pulses, which did not result in reaching the critical transmembrane potential, led only to pressing the vesicles together but did not cause fusion. For different pulse parameters (field strength and pulse duration) no qualitative difference in the fusion dynamics was observed.

In the absence of salt, the fusion typically occurs at several contact points as one can deduce by inspection of the optical micrographs (Fig. 1*b*). When the two vesicles fuse at more than two contact points and form more than two fusion necks, the coalescence of these fusion necks can lead to small, contact zone vesicles, which are visible as bright spots in the two last snapshots in Fig. 1*b*. Consider, e.g., three fusion necks that expand and touch each other in such a way that they enclose a roughly triangular segment of the contact zone. If the three necks are circular and have grown up to a diameter L_1, the enclosed contact zone segment will form a contact zone vesicle of radius $R_{czv} = 0.08\ L_1$ as follows from simple geometric considerations.

In the presence of salt ($\approx$1 mM NaCl) in the solution outside of the vesicles, the dc pulse induces cylindrical deformations as observed for single vesicles (30) (see first snapshot in Fig. 1*c*). The two vesicles are pushed together and form a flat contact zone in between (see Movie 4). In this case, no bright spots corresponding to enclosed vesicles are observed, from which we conclude that only one fusion neck or a small number of such necks has been formed initially. This conclusion is consistent with the observation that both membrane area and vesicle volume are conserved during these fusion processes and is confirmed by additional measurements using fluorescence microscopy (data not shown). All fusion events discussed in the following were obtained in the presence of salt, and for these events, no contact zone vesicles were observed. When the expanded fusion neck was located below or above the focal plane, the error in the determination of the neck diameter in the initial 300 μs was approximately $\pm$2 μm as indicated in Fig. 3*b*, but with further expansion, the fusion neck was in focus, thus bringing down the error to typical optical resolution of $\pm$0.25 μm.

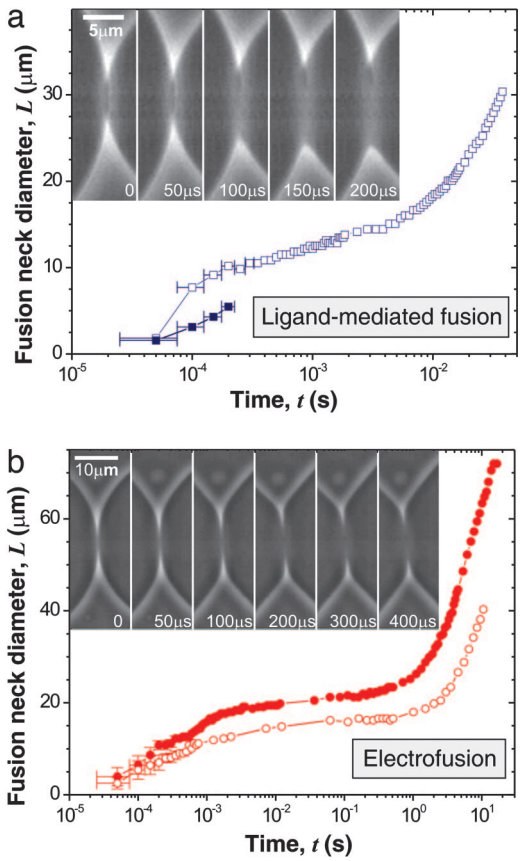

Fig. 3. Opening of the fusion neck. The fusion neck diameter, *L*, as a function of time, *t*, is plotted semilogarithmically for ligand-mediated fusion (*a*) and electofusion (*b*). The different symbols correspond to different vesicle couples (see *Methods* for details). The data set corresponding to the full squares in *a* represents a fusion event in which one of the two fusing vesicle ruptures before it completely merges with the second vesicle, which is why we show only data corresponding to the early stage of the fusion (before the membrane ruptures). The first dynamic regime that is characterized by rapid expansion of the fusion neck extends up to $\approx$300 μs for ligand-mediated fusion and up to $\approx$1 ms for electrofusion (compare with Fig. 5). (*Insets*) Snapshots with a magnified section of the fusion neck covering the time period from 0 to 400 μs.

Temporal Evolution of the Fusion Neck Diameter. For both ligand-induced fusion and electrofusion, we were able to record the opening of the fusion neck with an acquisition rate of 20,000 fps (Fig. 3). Detailed image analysis of the fusion zones shows that the opening of the fusion neck with a radius larger than $\approx$2 μm takes place within a couple of frames, e.g., within 100 μs (see Fig.

3 *Insets* and *Methods* for details on the data). A first inspection of Fig. 3 shows that the data obtained by the two different protocols exhibit a similar functional form for the fusion dynamics, i.e., for the fusion neck diameter, L, as a function of time, t. The time dependence of L already indicates two different dynamic regimes for both fusion protocols (see Fig. 5, which is published as supporting information on the PNAS web site).

A more detailed comparison of the data reveals that the range of neck diameters observed during the electrofusion process (Fig. 3*b*) is larger than during the ligand-mediated fusion (Fig. 3*a*). Likewise, the electrofusion data involve six orders of magnitude in time, whereas the ligand-mediated fusion data cover only three orders of magnitude in time. However, we will now show that the different ranges of neck diameters primarily reflect the difference in vesicle sizes, and all data sets for the earlier time regime collapse onto a single curve provided one rescales the neck diameter in an appropriate way. In addition, we show that the different behavior of the fusion neck diameter at later times is a result of the different tensions that the membranes experience during the later stage of the opening of the fusion neck.

The first dynamic regime corresponds to the early stage of the fusion neck opening and extends up to $\approx$300 μs for the ligand-mediated fusion process (see Fig. 3*a*) and up to $\approx$1 ms for the electrofusion process (see Fig. 3*b*). In the second dynamic regime, the neck opening slows down and the expansion velocity of the fusion neck, dL/dt, decreases by two orders of magnitude (note that this expansion velocity does not correspond to the slope of the curves in Fig. 3 because these plots are semilogarithmic).

To analyze the early stage of the fusion neck opening, we found it useful to plot the data in a variety of different ways. Because the fusion of larger vesicles would lead to the expansion of the fusion neck to larger diameter, in Fig. 4*a* the neck diameter L is rescaled by $(R_1 + R_2)$, where R_1 and R_2 are the radii of the two vesicles before they were brought into contact. Inspection of Fig. 4*a* shows that the data from the two fusion protocols collapse between 50 μs and $\approx$3 ms, i.e., during the early stage of the fusion neck opening.

The later stage of the expansion of the fusion neck covers the time evolution after a few milliseconds. In this regime, the expansion of the fusion neck proceeds much faster for ligand-mediated fusion than for electrofusion. This time shift is understandable if one considers the different constraints imposed on the vesicles during the two fusion protocols. For ligand-mediated fusion, each of the two vesicles is aspirated by a micropipette and the pressure is kept constant during the whole process, which implies that the membranes experience a large and essentially constant tension. After the fusion neck has been formed, it opens rapidly because the rim of the neck is pulled by the large membrane tension. On the other hand, after electrofusion, the tension within the membranes relaxes as the rim of the neck opens up.

It is instructive to use dimensional analysis to find an appropriate time scale, τ, for the later stage of the expansion of the fusion neck, i.e., after a few milliseconds. The driving force for this expansion is provided by the membrane tension, σ, whereas the hydrodynamic or Stokes friction is governed by the viscosity, η, of the aqueous solution to be displaced (we implicitly assume that Stokes friction dominates interbilayer friction as appropriate for length scales that exceed 0.5 μm). Our system is characterized by two well separated length scales, the membrane thickness, ℓ, and a typical vesicle size, R. We will choose $R = (R_1 + R_2)/2$, where R_1 and R_2 are the initial radii of the two vesicles as described. The only time scale, which one can obtain from a combination of the four variables σ, η, ℓ, and R, is given by $\tau = (\eta R/\sigma) f(\ell/R)$ with the dimensionless function $f(\ell/R)$. Because $\ell \ll R$, we can replace $f(\ell/R)$ by $f(0)$ and, thus, ignore corrections of order (ℓ/R).

For the electrofused vesicles relaxing at the bottom of the observation chamber, typical tensions should be in the range 0.05 to 0.1 mN/m as one can conclude from the visible shape fluctuations of the vesicle membranes (31). In contrast, the vesicle produced via ligand-mediated fusion is still aspirated by the micropipettes. The suction pressure applied by the micropipettes leads to a membrane tension of the order of 5 mN/m. For an effective vesicle radius $R \approx 20$ μm, e.g., we obtain the time scales $\tau = 4.4$ μs for the aspirated vesicles with $\sigma = 5$ mN/m, and $\tau = 0.44$ ms for the electrofused vesicles with $\sigma = 0.05$ mN/m. For each vesicle couple and tension conditions, we calculated the corresponding value of τ, which was used to define the rescaled time t/τ [see Fig. 4*a Inset* where we plot the rescaled fusion neck diameter, $L/(R_1 + R_2)$, as a function of t/τ]. This rescaling leads to a collapse of the two types of data sets for the later stage of the expansion of the fusion neck with $t/\tau > 10^3$. Thus, we conclude that both fusion protocols lead to essentially the same fusion dynamics.

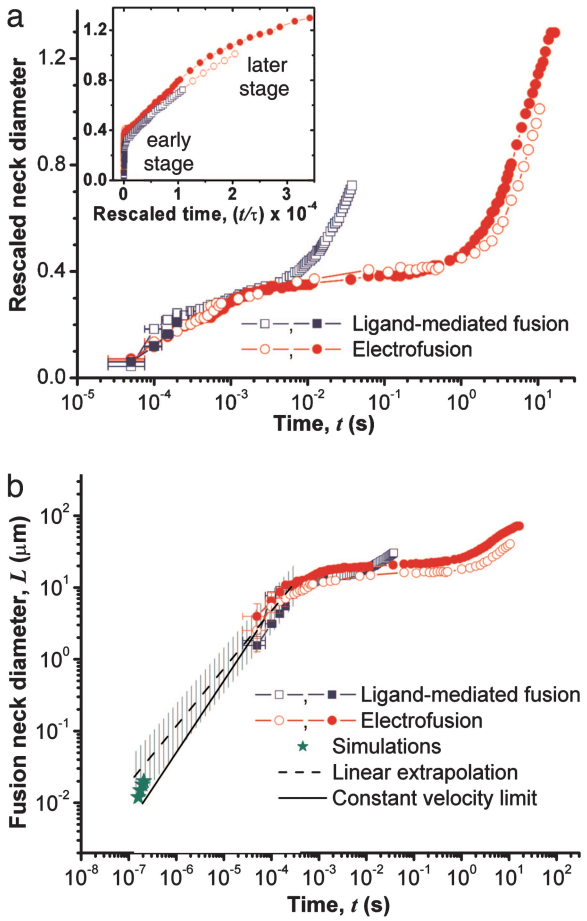

Fig. 4. Comparative data analysis of ligand-mediated fusion and electrofusion. (*a*) Rescaled fusion neck diameter $L/(R_1 + R_2)$ as a function of time t is plotted semilogarithmically. Note that the data sets collapse onto a single curve between 50 μs and 3 ms. (*Inset*) The rescaled fusion neck diameter as a function of the rescaled time t/τ (see text for definition of τ). The normalized data collapse onto a single curve for the later stages of the expansion of the fusion neck corresponding to $t/\tau > 10^3$. (*b*) Double logarithmic plot of the fusion neck diameter L as a function of time t. The solid line for $t < 50$ μs corresponds to an average expansion velocity of 5 cm/s as estimated from the first frames for the four fusion processes. Linear extrapolation of all data with $50 < t < 300$ μs leads to the dashed line that corresponds to an expansion velocity of 4 cm/s. The shaded stripe around this line indicates the fitting error as estimated by least-squares fitting. For comparison, simulation data from ref. 29 are also included. The latter data describe the opening of a single fusion neck for a small vesicle with a diameter of 28 nm and are consistent with the experimental data obtained here for the fusion neck expansion of giant vesicles.

Let us now go back to the early stages of the opening of the fusion neck. For the four fusion events displayed in Fig. 3, the fusion neck has attained an average diameter of ≈2.5 μm already after the first 50 μs. Let us first assume that the recorded fusion events have started from a single fusion pore or neck with an initial diameter of the order of 10 nm (i.e., somewhat larger than twice the membrane thickness). Because the measured neck diameter at $t = 50$ μs is much larger than 10 nm, it would imply an average expansion velocity of ≈5 cm/s during the first 50 μs. The main error for this estimate comes from the uncertainty for the choice of the initial frame, which represents the limit of our time resolution. To improve this estimate, we also use an extrapolation of the four data sets between 50 and 300 μs, which correspond to the first six frames. As shown in Fig. 4*b*, all four data sets have the same slope when plotted in a double-logarithmic manner. Because this slope is close to one, these data imply a roughly constant expansion velocity for the fusion neck between 50 and 300 μs, which is found to be ≈4 cm/s. The latter six-frame estimate is fairly close to, but somewhat smaller than, the first frame estimate of 5 cm/s. This finding is consistent with the general observation that the expansion velocity of the fusion neck decreases monotonically with time for all times.

It is important to note that essentially the same order of magnitude for the average expansion velocity is deduced if we assumed that the fusion process started with $N > 1$ fusion necks. These fusion necks would grow until they start to touch and coalesce. They would then create a coalesced neck of diameter L if each neck had grown up to $L/\sqrt{N}$. This implied an average expansion velocity of about $(5/\sqrt{N})$ cm/s, which is still of the same order of magnitude even if N were as large as 10.

Linear extrapolation of the data between 50 and 300 μs to smaller times leads to the shaded stripe in Fig. 4*b*. This extrapolation predicts that the formation of the fusion neck with a diameter of ≈10 nm should occur within a time period of ≈250 ns if the process started with a single neck or 250 $\sqrt{N}$ ns if it started with N such necks. Likewise, the first frame estimate leads to a time scale of ≈200 $\sqrt{N}$ ns for the initial formation of the fusion necks. It is quite remarkable that time scales of the order of 200 ns were also obtained from computer simulations for the formation of the initial fusion neck between a 28-nm vesicle and a 50-nm membrane segment under relatively large tension (32). In a somewhat speculative vein, we have included the simulation data for the time evolution of one such fusion event in Fig. 4*b*. Even though the size of the simulated vesicles is much smaller than the size of the giant vesicles studied here, the simulation data are quite consistent with both the first-frame and the six-frame estimate of our microscopy data.

In summary, we have been able to control and observe the fusion of lipid vesicles with a temporal resolution of 50 μs. We have used two different fusion protocols: fusion mediated by membrane-anchored β-diketone groups, which are cross-linked by europium ions, and fusion triggered by electroporation. In both cases, we found two different dynamic regimes for the expansion of the fusion neck. During the later stage of the fusion process, the neck expansion velocity slowed down by two orders of magnitude. Here, the dynamics were governed mainly by the displacement of the volume of liquid around the fusion neck between the fused vesicles. This conclusion is confirmed by the dimensional analysis provided in *Supporting Text*, which is published as supporting information on the PNAS web site.

The rapid initial expansion explains why it is so difficult to directly image the fusion process. If the fusion processes start with a single fusion neck, the average expansion velocity of the neck during the first 50 μs is found to be ≈5 cm/s, whereas the data points between 50 and 300 μs imply an expansion velocity of ≈4 cm/s. If the fusion processes started with N fusion necks, the average expansion velocity of the necks would be about $(5/\sqrt{N})$ cm/s.

The experimental approach used here can be applied to other fusion protocols as well. A particularly interesting example is provided by soluble *N*-ethylmaleimide-sensitive factor attachment protein receptor (SNARE)-induced fusion.

Methods

Preparation and Observation of Giant Unilamellar Vesicles. Giant unilamellar vesicles of L-α-phosphatidylcholine from egg yolk (Sigma, St. Louis, MO) were grown by using the electroformation method (33). The procedures used here are as in ref. 29. The membranes used for micropipette manipulation contained a small fraction (≤0.5 mol%) of amphiphilic β-diketone ligands (28). The vesicles were swelled in 0.2 M sucrose and subsequently diluted 40 times into 0.2 M glucose solution (some of the vesicle samples used for electrofusion were diluted in glucose solutions containing NaCl). The glucose/sucrose asymmetry creates a refraction index difference between the interior and the exterior of the vesicles. The latter enhances the contrast of the microscopy images (vesicle images appear dark on a bright background; see, e.g., Fig. 1). The observations were performed with an Axiovert135 microscope (Zeiss, Jena, Germany) equipped with ×20 and ×40 phase-contrast objectives and three micromanipulators (Sutter Instruments, Novato, CA and Narishige, Tokyo, Japan). The fusion events were recorded with a fast digital camera HG-100K (Redlake, Tucson, AZ) mounted on the microscope and connected to a personal computer. Image sequences were acquired at a frequency of up to 20,000 fps. The length of recording at this frequency did not exceed 2 s because of the limitation of the on-board memory of the camera as described. The illumination of the observation chamber was achieved with a mercury lamp HBO W/2. Sample heating caused by illumination was measured to be ≈2°C, and, thus, did not significantly affect the membrane properties. All measurements were performed at room temperature.

Fusion Protocol for Functionalized Membranes. The vesicle solution was placed in a specially designed chamber, which allows accommodation of three micropipettes: two for vesicle manipulation and one for ion injection (see *Supporting Text* for details). $EuCl_3$ was injected over a population of vesicles or directly into the area of contact between two giant vesicles being isolated by micropipettes. The concentration of $EuCl_3$ injected was varied between 1 μM and 1 mM, whereby all solutions were adjusted with glucose to be isoosmolar.

With either functionalized or pure lipid membranes, $EuCl_3$ was observed to induce adhesion between adjacent vesicles for the whole concentration range. Europium chloride concentrations <1 μM did not promote the fusion of the functionalized membranes. Concentrations >1 mM were not explored because they caused the membranes to rupture. The latter observation is intriguing because it suggests that the adsorption of Eu^{3+} on the membrane induces some tension. At higher concentrations this tension would reach the critical value of membrane lysis (≈7 mN/m), causing the vesicles to rupture. It is interesting to note that the injection of Ni^{2+} ions also leads to the adhesion of the functionalized vesicles, and sometimes to their rupture, but not to bilayer fusion.

The adhesion was found to be reversible once the concentration of $EuCl_3$ in the vicinity of the membranes decreased because of diffusion. The injected $EuCl_3$ was observed to induce fusion between adjacent membranes only in the case of functionalized vesicles. The range of β-diketone ligand concentrations that was explored in this study lies between 0.01 mol% (below this concentration no fusion was achieved) and 5 mol% (incorporation of more ligands in the bilayer was not possible). The fusion statistics were found to be essentially independent of the ligand concentration. Likewise, no dependence of the fusion statistics on the $EuCl_3$ concentration was detected.

The successful fusion events consisted of a prefusion stage, the

formation of a fusion neck, and the subsequent opening of this neck. During the prefusion stage, which lasted between 1 and 5 min after the injection of $EuCl_3$, the vesicles first adhered to each other, forming an extended contact area, and then the contact area slowly decreased until it was difficult to resolve with optical microscopy. During this prefusion stage, there was no exchange of lipid molecules between the two vesicles as demonstrated by fluorescent labeling of one of the membranes, implying that no hemifusion occurred. As explained before, it is currently not feasible to record the relatively long prefusion stage with a temporal resolution of 50 μs because of limitations imposed by the memory on the camera chip. Indeed, using the highest temporal resolution corresponding to 20,000 fps, one can record only $\approx$2 s.

When $EuCl_3$ was injected directly over a population of vesicles (>50 vesicles) fusion events were always observed. Repeating this observation on different preparations led to the statistics of having on average 30% of the vesicles fuse. The probability to induce a successful fusion event between two isolated vesicles using micropipettes is found to be reduced and of the order of 10% for those vesicle couples that do not rupture within a few seconds after the ion injection. As mentioned, we studied $\approx$50 such vesicle couples, 5 of which fused. We recorded three of these successful fusion events with a CCD camera and two with the fast digital camera. The data set presented with open blue squares in Fig. 3*a* ($R_1 = 25.4$ μm, $R_2 = 16.6$ μm) is obtained from one of these fast recordings (Movies 1 and 2 are from this fusion event). The second ligand-mediated fusion data set displayed with filled blue squares in Fig. 3*a* ($R_1 = 14.2$ μm, $R_2 = 8.5$ μm) is limited in duration because one of the vesicle ruptured $\approx$250 μs after fusion.

In the micropipette experiments, we monitored the membrane tension (34, 35) as obtained from the aspiration pressure and the Laplace equation. This tension varied between 0.01 and 7 mN/m but again was not observed to affect the fusion statistics in an essential way.

Electrofusion Protocol. The experimental chamber and the electroporation procedure have been described in detail (29); additional information is contained in *Supporting Text*. The applied field creates a transmembrane potential, which has its maximal value at the vesicle poles facing the electrodes. In these areas, macropores of diameter up to $\approx$5 μm are observed after $\approx$1 ms as demonstrated by the fluid that leaks out of the vesicles (see arrows on the first snapshots in Fig. 1 *b* and *c*). This leakage can be directly observed because the interior and the exterior solutions contain sucrose and glucose, respectively, and have sufficiently different refractive indices.

Applying the dc pulses (pulse strength from 1 to 4 kV/cm and pulse duration from 50 to 250 μs) to a couple of vesicles brought into contact leads to fusion. In the absence of salt, the fusion occurs at several contact points (see Movie 3). The coalescence of these necks can lead to small contact zone vesicles encapsulating glucose solution external to the two initial vesicles. As a consequence, these small vesicles appear as bright spots in the microscopy images (see the two last snapshots in Fig. 1*b*). One expects that these vesicles are interconnected by thin tethers because pinching the membrane off completely would require some additional energy input. It is interesting to note that this fusion-induced vesicle formation resembles the membrane processes during cell division when we look at them in a time-reversed manner. Indeed, during the initial stages of the division process, the cell accumulates membrane in the form of small vesicles that define the division plane and transform into two adjacent cell membranes.

In the presence of salt ($\approx$1 mM NaCl) in the solution outside of the vesicles, the dc pulse induced cylindrical deformations as observed for single vesicles (30) (see the first snapshot in Fig. 1*c*). The two vesicles were pushed together and formed a flat contact zone in between (see Movie 4). In this case, no bright spots corresponding to enclosed vesicles were observed from which we conclude that only one fusion neck or a small number of such necks had been formed initially.

The probability of successful fusion was $\approx$90%. In this case, the delay time between the applied electric pulse and the beginning of the electrofusion process is only a fraction of a millisecond, and it was, thus, easier to record this process with a fast camera. The acquired data on the neck diameter evolution were normalized by the average vesicle diameter as explained above. The fusion dynamics of 10 different vesicle couples was recorded and analyzed. The data set presented with filled red circles in Fig. 3*b* ($R_1 = 26.5$ μm, $R_2 = 29.0$ μm) is the one that is closest to the mean trend averaged from all of the data sets. The second electrofusion data set displayed with open red circles in Fig. 3*b* ($R_1 = 20.3$ μm, $R_2 = 22.6$ μm) represents one of the farthest deviations observed.

We thank M.-J. Brienne (Collège de France, Paris, France) for the synthesis of the β-diketone molecules and J. Shillcock for useful discussions. This work was supported by the Deutsche Forschungsgemeinschaft via the French–German Network.

1. Fischer A, Franco A, Oberholzer T (2002) *Chem Biol Chem* 3:409–417.
2. Noireaux V, Libchaber A (2004) *Proc Natl Acad Sci USA* 101:17669–17674.
3. Lipowsky R, Dimova R (2003) *J Phys Condens Matter* 15:S31–S45.
4. Dietrich C, Bagatolli LA, Volovyk ZN, Thompson NL, Levi M, Jacobson K, Gratton E (2001) *Biophys J* 80:1417–1428.
5. Baumgart T, Hess ST, Webb WW (2003) *Nature* 425:821–824.
6. Veatch SL, Keller SL (2003) *Biophys J* 85:3074–3083.
7. Kahya N, Scherfeld D, Bacia K, Poolman B, Schwille P (2003) *J Cell Biol* 278:28109–28115.
8. Jahn R, Grubmüller H (2002) *Curr Opin Cell Biol* 14:488–495.
9. Tamm LK, Crane J, Kiessling V (2003) *Curr Opin Struct Biol* 13:453–466.
10. Chandler D, Heuser J (1980) *Cell Biol* 86:666–674.
11. Schneider SW, Sritharan KC, Geibel JP, Oberleithner H, Jena BP (1997) *Proc Natl Acad Sci USA* 94:316–321.
12. Llinas R, Steinberg IZ, Walton K (1981) *Biophys J* 33:323–351.
13. Lindau M, de Toledo GA (2003) *Biochim Biophys Acta* 1641:167–173.
14. Hafes I, Kisler K, Berberian K, Dernick G, Valero V, Yong MG, Craighead HG, Lindau M (2005) *Proc Natl Acad Sci USA* 102:13879–13884.
15. Biswas B, Guha S (1999) *Bioelectrochem Bioenerg* 48:435–440.
16. Yang L, Huang HW (2002) *Science* 297:1877–1879.
17. Menger FM, Balachander N (1992) *J Am Chem Soc* 114 5862–5864.
18. Richard A, Marchi-Artzner V, Lalloz M-N, Brienne M-J, Artzner F, Gulik-Krzywicki T, Guedeau-Boudeville M-A, Lehn J-M (2004) *Proc Natl Acad Sci USA* 101:15279–15284.
19. Zimmermann U (1986) *Rev Physiol Biochem Pharmacol* 105:176–256.
20. Neumann E, Sowers A, Jordan C (1989) *Electroporation and Electrofusion in Cell Biology* (Plenum, New York).
21. Chang DC, Chassey BM, Saunders JA, Sowers AE (1992) *Guide to Electroporation and Electrofusion* (Academic, New York).
22. Jahn R, Lang T, Südhof TC (2003) *Cell* 112:519–533.
23. Söllner T, Whiteheart SW, Brunner M, Erjument-Bromage H, Gerromanos S, Tempst P, Rothman JE (1993) *Nature* 362:318–324.
24. Fix M, Melia TJ, Jaiswal JK, Rappoport JZ, You D, Söllner TH, Rothman JE, Simon SM (2004) *Proc Natl Acad Sci USA* 101:7311–7316.
25. Hu C, Ahmed M, Melia TJ, Söllner TH, Mayer T, Rothman JE (2003) *Science* 300:1745–1749.
26. Peters C, Andrews PD, Stark MJR, Cesaro-Tadic S, Glatz A, Podtelejnikov A, Mann M, Mayer A (1999) *Science* 285:1084–1087.
27. Marchi-Artzner V, Gulik-Krzywicki T, Guedeau-Boudeville M-A, Gosse C, Sanderson JM, Dedieu J-C, Lehn J-M (2001) *ChemPhysChem* 2:367–376.
28. Marchi-Artzner V, Brienne M-J, Gulik-Krzywicki T, Dedieu J-C, Lehn J-M (2004) *Chem Eur J* 10:2342–2350.
29. Riske KA, Dimova R (2005) *Biophys J* 88:1143–1155.
30. Riske KA, Dimova R (2006) *Biophys J* 91:1778–1786.
31. Lipowsky R, Sackmann E (1995) *Structure and Dynamics of Membranes* (Elsevier, Amsterdam).
32. Shillcock JC, Lipowsky R (2005) *Nat Mater* 4:225–228.
33. Angelova MI, Dimitrov DS (1986) *Faraday Discuss Chem Soc* 81:303–311.
34. Evans E, Rawicz W (1990) *Phys Rev Lett* 17:2094–2097.
35. Merkel R, Nassoy P, Leung A, Ritchie K, Evans E (1999) *Nature* 397:50–53.